Supplementary Information:

Future methane, hydroxyl, and their uncertainties: key climate and emission parameters for future predictions

Christopher D. Holmes [1*], Michael J. Prather [1], Amund O. Søvde [2], Gunnar Myhre [2]

[1] Department of Earth System Science, University of California, Irvine, CA 92697-3100 USA

[2] Center for International Climate and Environmental Research (CICERO), Oslo, Norway

[*] Correspondence to cdholmes@uci.edu

Methyl chloroform decay rate and its uncertainty

The AGAGE network consists of 5 sites, each of which makes measurements every 20 minutes, with analysis and calibration done on site. In the NOAA network, flasks are filled 1-4 times monthly and analyzed in a central laboratory in Boulder, Colorado. To avoid pollution influences, flasks are filled when winds blow from a clean sector. In the AGAGE network polluted samples are identified as anomalously high MCF concentrations and removed from analysis.

Both networks provide monthly average data for each of their sites, which we use here (NOAA: (IPCC, 2007), accessed Jan 5, 2012; AGAGE: (Prather et al., 2001), accessed April 4, 2012). For the NOAA network, we use data from the same 9 sites as Montzka et al. (2011) (South Pole; Cape Grim, Australia; Cape Matatula, American Samoa; Alert, Canada; and United States sites at Mauna Loa, Hawaii; Niwot Ridge, Colorado; KLEF tower, Minnesota; and Barrow, Alaska). All 5 AGAGE sites are used here analysis (Cape Grim, Australia; Cape Matatula, American Samoa; Ragged Point, Barbados; Trinidad Head, United States; and Mace Head, Ireland). NOAA data are truncated at December 2007 due to later quality issues (S. Montzka, pers. comm.).

Our method for calculating the global MCF decay rate differs from that of Montzka et al. (2011). Montzka et al. first constructed a global mean tropospheric MCF abundance from a weighted average of the sites, then calculated the global decay rate using the same formula we have applied to each site individually. We find our method to be much less sensitive to site selection and methods for filling missing data, but our global mean decay rates and their anomalies are, nevertheless, very similar, as shown in Figure S1. Differences are always less than 1% after 2000, but are as large as 2% in early 1998, due to more frequent data gaps in the early period.

Future tropospheric temperature and water vapor

The parametric model for $\tau_{CH4\times OH}$ requires atmospheric temperature and water vapor as inputs, averaged over 40°S-40°N and from the surface to 400 hPa. These input data must be consistent with other scenario emission data, which are taken from RCP 8.5 in this work. Averages over the required region, where 80% of methane oxidation occurs, are not readily available from CMIP5

models. Therefore, for our future methane predictions, we derive atmospheric temperature and water vapor from sea-surface temperature (SST) in the CMIP5, using historical correlations between these climate variables.

Figure S3 shows strong correlations between historical (1979-2010) SST and tropospheric temperatures for the region of fast methane loss. These correlations are robust against different meteorological analysis products (R^2=0.7 to 0.8). Using MERRA data (Bosilovich et al., 2011) since 1979, the slope of atmosphere vs. sea-surface temperatures is 1.28 ± 0.1. ECMWF data (cycle 36r1, (Prather et al., 2012)) since 1997 yield a statistically indistinguishable value. Using other SST data (e.g. Reynolds et al., 2002) does not alter the result (not shown). A slope greater than 1 is expected from physical princples and Santer et al. (2005) found a similar ratio of 1:1.3 for multidecadal trends in surface temperature vs. lower tropospheric temperature.

Water vapor mixing ratio can be calculated from atmospheric temperature using standard vapor pressure formulas (e.g. Eq. 2.61 Jacobson, 2005), assuming constant relative humidity. Figure S4 shows that the calculated water vapor is highly correlated with reanalysis water vapor (R^2 = 0.7-0.8) with a slope of 1.51 ± 0.18 when the calculations are based on SST. The slope deviates from 1:1 because both temperature and water vapor are averaged over a large region (40°S-40°N, surface to 400 hPa), while vapor pressure formulas strictly apply only to homogeneous regions.

An ensemble of 34 CMIP5 models provide SST predictions for RCP 8.5 climate (Climate Explorer, http://climexp.knmi.nl/, accessed July 18, 2012). We calculate future atmospheric temperature, $T_i(t)$ in each model i to be

$$T_i(t) = T_0 * [1 + a_1 * (SST_i(t) / SST_i(t_0) - 1)],$$

Where $SST_i(t)$ is the model's SST, t_0 = 2010, T_0 = 278.5 K (ECMWF 2000-2009 mean), and a_1 = N(1.3, 0.1) is a normally distributed random number that accounts for uncertainty in the historical fit between atmospheric temperature and SST. Future water vapor mixing ratio, $q_i(t)$, in the same model is

$$q_i(t) = p(T_0) + a_2 * [p(T_i(t)) - p(T_0)],$$

where $p(T)$ is the saturation vapor pressure at temperature T and a_2 = N(1.5, 0.2) accounts for uncertainty in the historical fit between water vapor and its SST-derived estimate. Through 10^5 monte carlo realizations of a_1 and a_2 we estimate uncertainty in atmospheric future temperature and water vapor in RCP 8.5.

Figure S5 shows the air temperature and water vapor changes inferred from the SST data. While SST increases 3.2 ± 0.6 K by 2100 in RCP 8.5, atmospheric temperatures increase 4.0 ± 0.9 K and water vapor increases 38.2 ± 8.9 % over the same period.

References

Bosilovich, M. G., Robertson, F. R. and Chen, J.: Global Energy and Water Budgets in MERRA, J Climate, 24(22), 5721–5739, doi:10.1175/2011JCLI4175.1, 2011.

Jacobson, M. Z.: Fundamentals of Atmospheric Modeling, 2nd ed. Cambridge University Press, Cambridge, UK. 2005.

Montzka, S. A., Krol, M., Dlugokencky, E., Hall, B., Joeckel, P. and Lelieveld, J.: Small Interannual Variability of Global Atmospheric Hydroxyl, Science, 331(6013), –, doi:10.1126/science.1197640, 2011.

88 Reynolds, R., Rayner, N., Smith, T., Stokes, D. and Wang, W.: An improved in situ and satellite
89 SST analysis for climate, J Climate, 15(13), 1609–1625, 2002.

90 Santer, B., Wigley, T., Mears, C., Wentz, F., Klein, S., Seidel, D., Taylor, K., Thorne, P.,
91 Wehner, M., Gleckler, P., Boyle, J., et al.: Amplification of surface temperature trends and
92 variability in the tropical atmosphere, Science, 309(5740), 1551–1556,
93 doi:10.1126/science.1114867, 2005.

94

95

96

Table S1: CTM simulations[a]

Description or perturbed variable	Perturbation		
	Magnitude	Region	Duration, y
Control simulation, no perturbations	-	-	UCI, CTM3: 13 GEOS-Chem MERRA: 13 GEOS-5: 6
Air temperature in chemistry solver	+1 K	global[c]	3
Water vapor in chemistry solver	+5 %	global[c]	3
Ozone column in photolysis code	+1 %	40°S-40°N	3
Biomass burning emissions	+5 %	global	3 (13 for UCI)
Lightning NOx emissions	+20 %	global	3
Anthropogenic NOx emissions over land	+7.8 %[b]	global	3
Anthropogenic NOx emissions from ships	+14.4%[b]	global	3
CH_4 abundance	+5 %	global	13
Convective mass flux	–20 %	global	3 (UCI only)
Cloud optical depth (all clouds) in photolysis code	+5 %	global	3 (UCI only)
Cloud optical depth (ice clouds) in photolysis code	+5 %	global	3 (UCI only)
Cloud optical depth (liquid clouds) in photolysis code	+5 %	global	3 (UCI only)

[a] Each variable is perturbed in a separate simulation. All perturbation tests are compared against a control run from the same CTM. GEOS-Chem perturbation tests use GEOS-5 meteorology only.
[b] This magnitude is the projected increase during the period 2000-2030 in RCP 8.5.
[c] In Oslo CTM3, temperature and water vapor perturbations are applied only to grid levels below 200 hPa to avoid confounding effects on stratospheric chemistry.

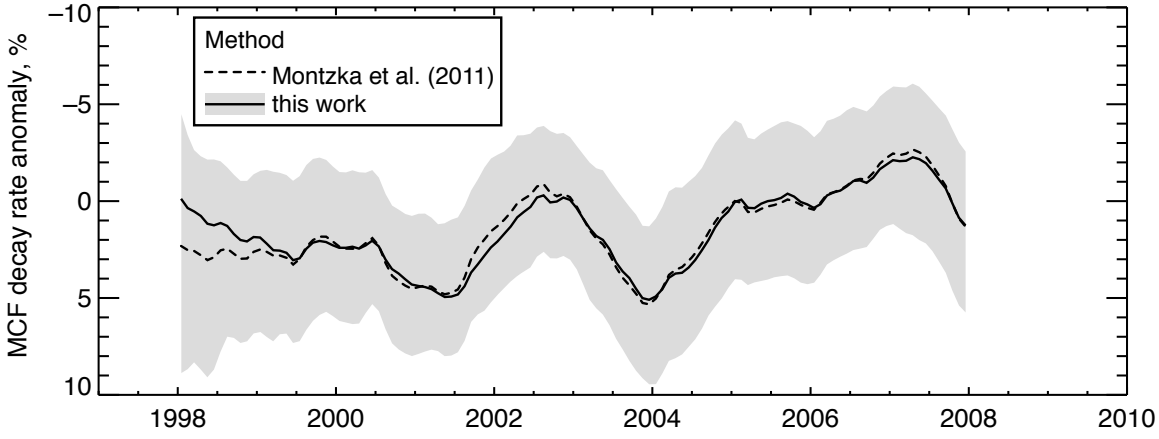

Figure S1. Global decay rate anomalies for methyl chloroform, calculated from NOAA data using two methods. Results from this work are compared to previously published work of Montzka et al. (2011). Shading shows the uncertainty, given by the 16th to 84th percentile range of decay rates across stations within each network, calculated in this work.

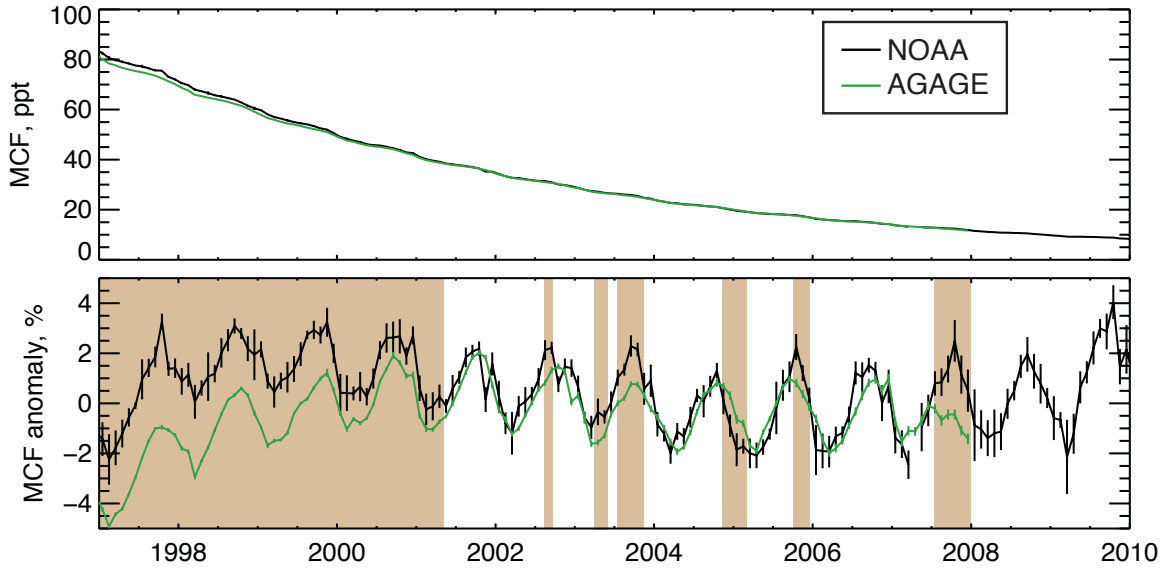

Figure S2. Methyl chloroform (MCF) abundance at the Cape Grim, Australia, as measured by the NOAA and AGAGE stations. Anomalies (bottom) are calculated with respect to a single decaying exponential reference curve that is fitted to all observations from both stations after 2000. Vertical lines show standard errors in the monthly mean abundances. Shading highlights episodes were the NOAA and AGAGE monthly means differ by more than their standard errors for 2 or more consecutive months.

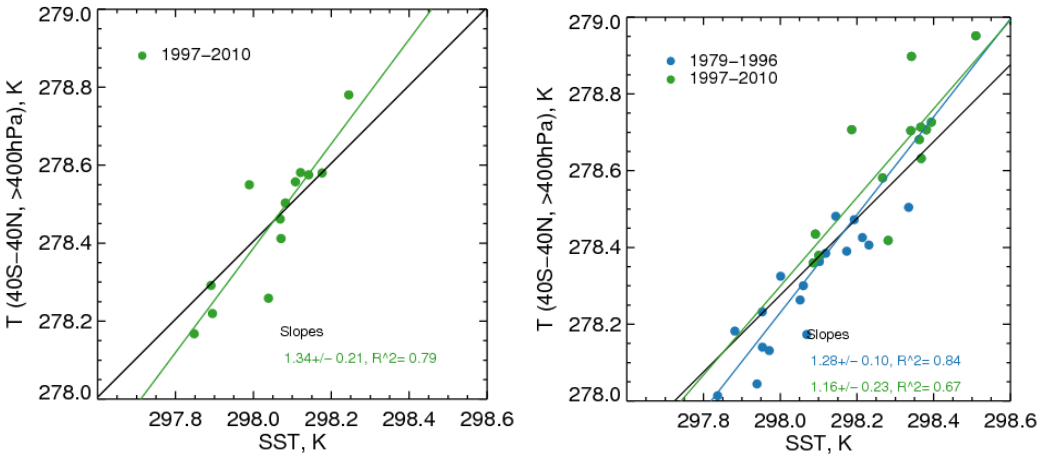

Figure S3. Annual mean tropospheric temperature in the region of rapid methane loss (40°S-40°N, surface to 400hPa) and annual mean SST (40°S-40°N) for ECMWF (left) and MERRA (right) meteorological analyses. Black line shows 1:1 relation. Blue and green lines are ordinary least squares regressions for all years and 1997-2010, respectively.

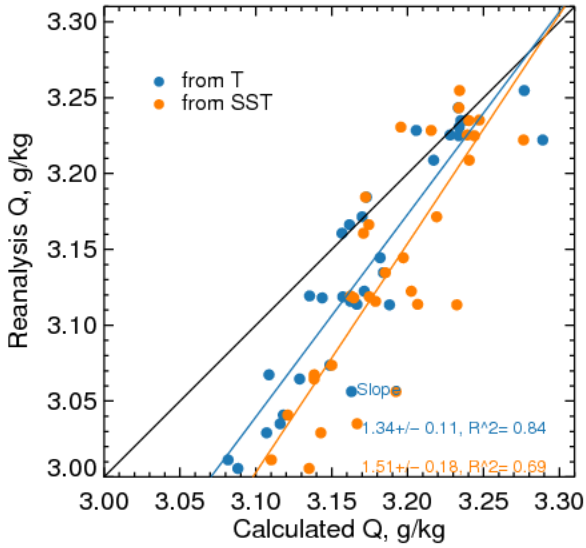

Figure S4. Water vapor mixing ratio from MERRA reanalysis (1979-2009) and calculated from temperature. Calculations are based on either SST (orange dots) or atmospheric temperature (blue dots) from MERRA reanalysis, using standard vapor pressure formulas, assuming constant relative humidity. Water vapor and SST are averaged over 40°S-40°N. Atmospheric temperatures are additionally averaged from the surface to 400hPa.

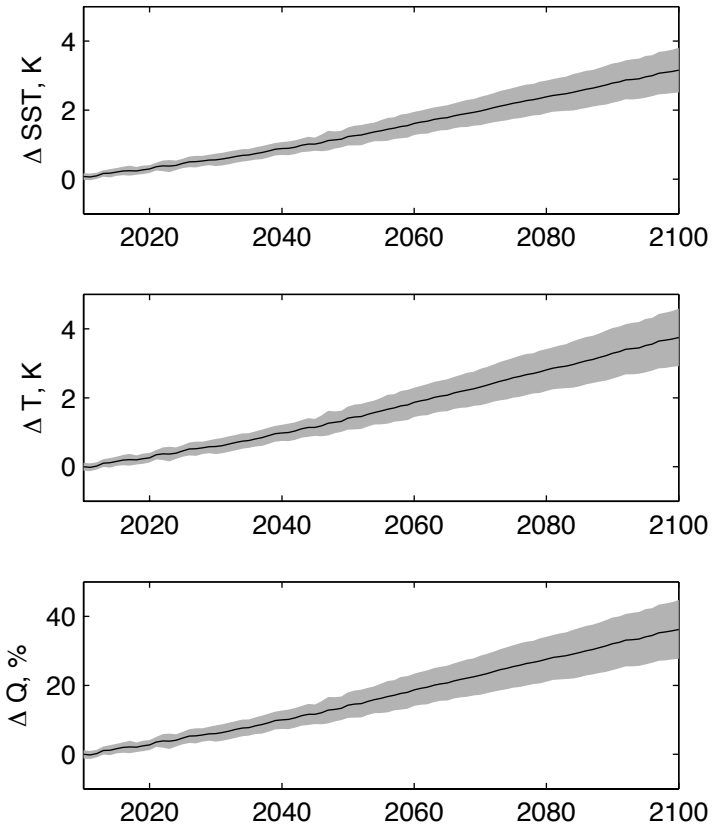

Figure S5. Predicted anomalies in SST (top), atmospheric temperature (middle), and water vapor (bottom) for RCP 8.5. SSTs are from an ensemble of 34 CMIP5 models, while other variables are derived from SSTs, as described in this supplement. All variables are averages over 40°S-40°N and atmospheric data are averaged from the surface to 400 hPa. Shading shows 1σ uncertainty.

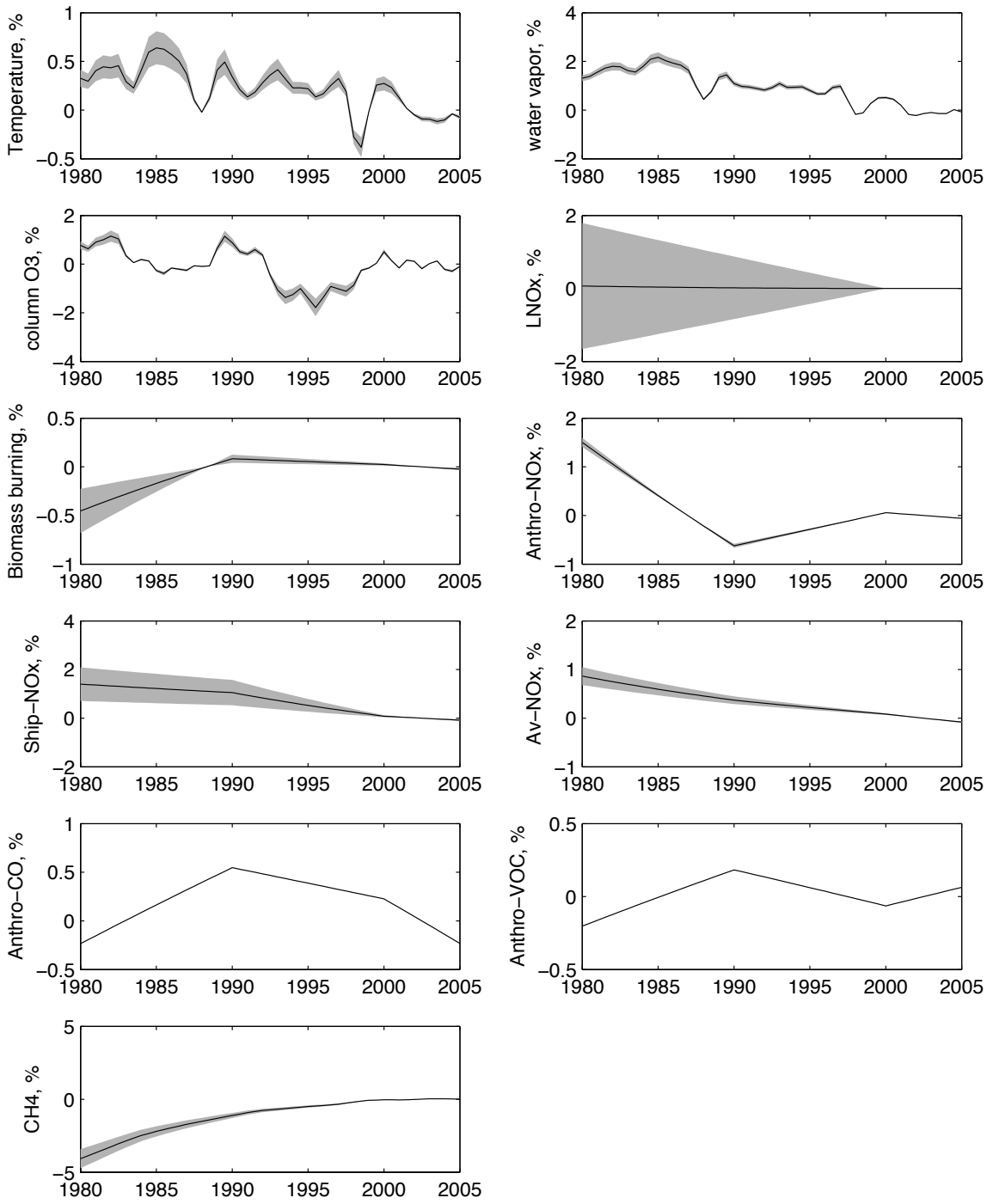

Figure S6. Contributions of climate and emission forcing variables to changes in $\tau_{CH4\times OH}$ since 1980. The sum of all contributions equals the change in lifetime shown in Figure 4.